Secure Transmission in Uplink C-RAN Systems with RSMA, NOMA, and SDMA

Yao Zhang*†, Yongxu Zhu†, Dongming Wang†, Wenchao Xia‡, Weidang Lu§, and Bo Tan¶‖
*School of Communications Engineering, Hangzhou Dianzi University, Hangzhou 310018, China
†National Mobile Communications Research Laboratory, Southeast University, Nanjing, 210096, China
‡Department of Wireless Communication Key Lab of Jiangsu Province, Nanjing University of Posts and Telecommunications, Nanjing 210003, China
§College of Information Engineering, Zhejiang University of Technology, Hangzhou 310023, China
¶Department of Electronic and Electrical Engineering, University College London, London WC1E 7JE, UK
‖Tampere Wireless Research Centre, Faculty of Information Technology and Communication Sciences, Tampere University, Finland
Corresponding Author: Yongxu Zhu Email: yongxu.zhu@seu.edu.cn

***Abstract*—This paper investigates secure transmission in the uplink of a cloud radio access network (C-RAN) system incorporating rate-splitting multiple access (RSMA), non-orthogonal multiple access (NOMA), and space-division multiple access (SDMA). We derive closed-form expressions for the secrecy spectral efficiency (SSE) under Rician fading channels with imperfect channel state information. The security performance is comprehensively analyzed across diverse system parameters, including the density of access points, user distribution, line-of-sight (LoS) component intensity, and multiple access schemes. Numerical results corroborate the theoretical analysis and demonstrate that RSMA achieves superior SSE performance compared to conventional NOMA and SDMA schemes, particularly in scenarios characterized by severe inter-user interference and strong LoS components.**

***Index Terms*—Cloud radio access network, rate-splitting multiple access, secrecy performance analysis.**

I. Introduction

Owing to its capability to provide uniformly high-quality service while significantly enhancing the spectral and energy efficiencies, cloud radio access network (C-RAN) has emerged as a promising technology for future communications [1]. Previous studies on C-RAN systems have predominantly focused on space-division multiple access (SDMA), which employs multi-user precoding and reception based on current channel state information (CSI) to suppress inter-user interference (IUI) [2]. However, SDMA's effectiveness is substantially constrained by CSI accuracy, resulting in degraded performance in environments characterized by high interference levels.

To address these limitations, non-orthogonal multiple access (NOMA) has emerged as an alternative approach that achieves enhanced spectral efficiency (SE) compared to SDMA by managing interference through successive interference cancellation (SIC) at the receiver [3]. However, NOMA's effectiveness is contingent upon specific conditions, including channel alignment and substantial disparities in channel gains. The inherent challenges of IUI management in both SDMA and NOMA have motivated the development of rate-splitting multiple access (RSMA) [4]. RSMA implements a message-splitting strategy wherein each user's data is partitioned into multiple independent streams, which are independently encoded and reconstructed via SIC at the receiver. By virtue of its adaptive interference management capabilities and operational flexibility, RSMA presents a more robust transmission framework compared to conventional multiple access schemes, making it particularly suitable for C-RAN deployments.

The inherent broadcast nature of wireless channels renders C-RAN systems vulnerable to eavesdropping attacks, necessitating the implementation of physical layer security techniques to ensure secure transmission regardless of eavesdroppers' (Eves) capabilities [5]. While existing literature [6–8] has extensively investigated secure transmission in SDMA-based C-RAN systems, the potential security advantages of RSMA remain largely unexplored. Given RSMA's demonstrated superiority in spectral efficiency through enhanced inter-user interference management, its application to security enhancement in C-RAN systems warrants investigation. Our previous work [9] established RSMA's superior SSE performance in downlink C-RAN systems with imperfect channel state information compared to SDMA. However, that analysis excluded NOMA comparisons and uplink scenarios. The security of uplink transmission is particularly critical due to users' hardware constraints, specifically limited antenna configurations and transmission power, which may compromise the confidentiality of information transmission to access points (APs).

To the best of our knowledge, no prior work has investigated the SSE of an uplink C-RAN system with RSMA, nor has there been a comprehensive comparison of RSMA, NOMA, and SDMA in terms of SSE. This gap in the existing literature underscores the need for a detailed analysis of these multiple access schemes in the context of secure uplink transmissions. This work addresses the aforementioned research gaps by analyzing the SSE in the uplink of C-RAN systems employing RSMA, NOMA, and SDMA. The analysis incorporates practical considerations of imperfect CSI and derives closed-form SSE expressions under correlated Rician fading channels.

This work was supported in part by the Zhejiang Provincial Natural Science Foundation of China under Grant LQ23F010010 and in part by the open research fund of National Mobile Communications Research Laboratory of Southeast University under Grant 2025D11.

Through extensive numerical evaluations, we demonstrate that RSMA exhibits superior secrecy performance compared to conventional NOMA and SDMA schemes across diverse system configurations. This performance advantage becomes particularly pronounced in scenarios characterized by high LoS probability and intense inter-user interference, thereby providing valuable insights for the design of secure multiple access systems.

II. System Model

In this work, we study the uplink transmission of a C-RAN system, wherein M APs, each deployed with N antennas, collaboratively serve K single-antenna users through RSMA, SDMA, and NOMA techniques. Under the NOMA paradigm, the K users are partitioned into J clusters, with each cluster comprising T users, satisfying $K = JT$. For notational clarity, we denote the t-th user in the j-th cluster as user jt. Moreover, the system incorporates a malicious Eve, equipped with L antennas, aiming to intercept legitimate user transmissions. The sets of APs, users, clusters, and users within each cluster are represented by $\mathcal{M} = \{1, \ldots, M\}$, $\mathcal{K} = \{1, \ldots, K\}$, $\mathcal{J} = \{1, \ldots, J\}$, and $\mathcal{T} = \{1, \ldots, T\}$, respectively.

A. System Model

We employ the correlated Ricean fading channel model to characterize the channel responses [10]. As a result, the wireless channel between AP m and user k is depicted as

$$\boldsymbol{g}_{mk} \in \mathbb{C}^N \sim \mathcal{N}_{\mathbb{C}} \left(e^{i\theta^{\mathrm{P}}_{mk}} \sqrt{\beta_{mk} K_{mk}} \bar{\boldsymbol{g}}_{mk}, \beta_{mk} \tilde{\boldsymbol{R}}_{mk} \right), \quad (1)$$

where $\bar{\boldsymbol{g}}_{mk}$ represents the LoS component of $\boldsymbol{g}_{mk}$ and $\beta_{mk} = \frac{\zeta_{mk}}{K_{mk}+1}$ is the effective channel fading, where ζ_{mk} is the large-scale fading coefficient. Additionally, θ^{P}_{mk} signifies the LoS phase shift, K_{mk} represents the Ricean factor, and $\tilde{\boldsymbol{R}}_{mk}$ means the spatial correlation matrix at AP m. In addition, the channel vector between Eve and user k is given as

$$\boldsymbol{g}_{k,\mathrm{e}} \in \mathbb{C}^L \sim \mathcal{N}_{\mathbb{C}} \left(e^{i\theta^{\mathrm{P}}_{k,\mathrm{e}}} \sqrt{\beta_{k,\mathrm{e}} K_{k,\mathrm{e}}} \bar{\boldsymbol{g}}_{k,\mathrm{e}}, \beta_{k,\mathrm{e}} \tilde{\boldsymbol{R}}_{k,\mathrm{e}} \right), \quad (2)$$

where $\beta_{k,\mathrm{e}} = \frac{\zeta_{k,\mathrm{e}}}{K_{k,\mathrm{e}}+1}$ with $\zeta_{k,\mathrm{e}}$ and $K_{k,\mathrm{e}}$ representing the large-scale fading coefficient and Ricean factor. $\bar{\boldsymbol{g}}_{k,\mathrm{e}}$, $\theta^{\mathrm{P}}_{k,\mathrm{e}}$ and $\tilde{\boldsymbol{R}}_{k,\mathrm{e}}$ respectively denote the LoS component, LoS phase shift, and spatial correlation matrix of Eve to user k.

By applying the above modeling approach, we can respectively establish the channel vectors from user jt to AP m and to Eve, resulting in

$$\boldsymbol{g}_{mjt} \in \mathbb{C}^N \sim \mathcal{N}_{\mathbb{C}} \left(e^{i\theta^{\mathrm{P}}_{mjt}} \sqrt{\beta_{mjt} K_{mjt}} \bar{\boldsymbol{g}}_{mjt}, \beta_{mjt} \tilde{\boldsymbol{R}}_{mjt} \right), \quad (3)$$

and

$$\boldsymbol{g}_{jt,\mathrm{e}} \in \mathbb{C}^L \sim \mathcal{N}_{\mathbb{C}} \left(e^{i\theta^{\mathrm{P}}_{jt,\mathrm{e}}} \sqrt{\beta_{jt,\mathrm{e}} K_{jt,\mathrm{e}}} \bar{\boldsymbol{g}}_{jt,\mathrm{e}}, \beta_{jt,\mathrm{e}} \tilde{\boldsymbol{R}}_{jt,\mathrm{e}} \right), \quad (4)$$

where the parameters in (3) and (4) have the same meanings as those in (1) and (2).

B. Channel Estimation for RSMA and SDMA

Denote $\boldsymbol{\phi}_k \in \mathbb{C}^{\tau_{\mathrm{p}}}$ as the unit-variance pilot assigned to user k, satisfying $\boldsymbol{\Phi}^H_{k'} \boldsymbol{\phi}_k = 0, \forall k' \notin \mathcal{P}_k$ and $\boldsymbol{\phi}^H_{k'} \boldsymbol{\phi}_k = 1, \forall k' \in \mathcal{P}_k$, where $\mathcal{P}_k$ represents the set of user indices that reuse $\boldsymbol{\phi}_k$[1]. Since channel estimation is a well-established and standardized topic in C-RAN systems [4, 10], detailed derivations are omitted for brevity. Instead, we directly present the MMSE estimates of $\boldsymbol{g}_{mk}$ and $\hat{\boldsymbol{g}}_{k,\mathrm{e}}$ in the form of lemmas.

Lemma 1: The MMSE estimations of $\boldsymbol{g}_{mk}$ and $\boldsymbol{g}_{k,\mathrm{e}}$ are Gaussian distributed and take the form of

$$\hat{\boldsymbol{g}}_{mk} \sim \mathcal{N}_{\mathbb{C}} \left(e^{i\theta^{\mathrm{P}}_{mk}} \underbrace{\sqrt{\beta_{mk} K_{mk}} \bar{\boldsymbol{g}}_{mk}}_{\bar{\boldsymbol{h}}_{mk}}, \underbrace{\tau_{\mathrm{p}} \rho_{\mathrm{p}} \boldsymbol{R}_{mk} \boldsymbol{\Psi}^{-1}_{mk} \boldsymbol{R}^H_{mk}}_{\boldsymbol{Q}_{mk}} \right), \quad (5)$$

and

$$\hat{\boldsymbol{g}}_{k,\mathrm{e}} \sim \mathcal{N}_{\mathbb{C}} \left(e^{i\theta^{\mathrm{P}}_{k,\mathrm{e}}} \underbrace{\sqrt{\beta_{k,\mathrm{e}} K_{k,\mathrm{e}}} \bar{\boldsymbol{g}}_{k,\mathrm{e}}}_{\bar{\boldsymbol{h}}_{k,\mathrm{e}}}, \underbrace{\tau_{\mathrm{p}} \rho_{\mathrm{p}} \boldsymbol{R}_{k,\mathrm{e}} \boldsymbol{\Psi}^{-1}_{k,\mathrm{e}} \boldsymbol{R}^H_{k,\mathrm{e}}}_{\boldsymbol{Q}_{k,\mathrm{e}}} \right), \quad (6)$$

where ρ_{p} is the training power, σ^2 is the power of the additive white Gaussian noise (AWGN), $\boldsymbol{\Psi}_{mk} = \tau_{\mathrm{p}} \rho_{\mathrm{p}} \sum_{k' \in \mathcal{P}_k} \boldsymbol{R}_{mk'} + \sigma^2 \boldsymbol{I}_N$, $\boldsymbol{R}_{mk} = \beta_{mk} \tilde{\boldsymbol{R}}_{mk}$, $\boldsymbol{\Psi}_{k,\mathrm{e}} = \tau_{\mathrm{p}} \rho_{\mathrm{p}} \sum_{k' \in \mathcal{P}_k} \boldsymbol{R}_{k',\mathrm{e}} + \sigma^2 \boldsymbol{I}_L$, and $\boldsymbol{R}_{k,\mathrm{e}} = \beta_{k,\mathrm{e}} \tilde{\boldsymbol{R}}_{k,\mathrm{e}}$.

C. Channel Estimation for NOMA

NOMA enables users within the same cluster to share the same pilot, denoted as $\boldsymbol{\varphi}_j \in \mathbb{C}^J$. As a result, only J mutually orthogonal pilots are required for NOMA systems. Following a similar approach to Section II-B, we present the MMSE estimations of $\boldsymbol{g}_{mjt}$ and $\boldsymbol{g}_{jt,\mathrm{e}}$ as in Lemma 2.

Lemma 2: The MMSE estimations of $\boldsymbol{g}_{mjt}$ and $\boldsymbol{g}_{jt,\mathrm{e}}$ follow a Gaussian distribution and are given as

$$\hat{\boldsymbol{g}}_{mjt} \sim \mathcal{N}_{\mathbb{C}} \left(e^{j\theta^{\mathrm{P}}_{mjt}} \underbrace{\sqrt{\beta_{mjt} K_{mjt}} \bar{\boldsymbol{g}}_{mjt}}_{\bar{\boldsymbol{h}}_{mjt}}, \underbrace{\tau_{\mathrm{p}} \rho_{\mathrm{p}} \boldsymbol{R}_{mjt} \boldsymbol{\Psi}^{-1}_{mjt} \boldsymbol{R}^H_{mjt}}_{\boldsymbol{Q}_{mjt}} \right), \quad (7)$$

and

$$\hat{\boldsymbol{g}}_{jt,\mathrm{e}} \sim \mathcal{N}_{\mathbb{C}} \left(e^{i\theta^{\mathrm{P}}_{jt,\mathrm{e}}} \underbrace{\sqrt{\beta_{jt,\mathrm{e}} K_{jt,\mathrm{e}}} \bar{\boldsymbol{g}}_{jt,\mathrm{e}}}_{\bar{\boldsymbol{h}}_{jt,\mathrm{e}}}, \underbrace{J \rho_{\mathrm{p}} \boldsymbol{R}_{jt,\mathrm{e}} \boldsymbol{\Psi}^{-1}_{jt,\mathrm{e}} \boldsymbol{R}^H_{jt,\mathrm{e}}}_{\boldsymbol{Q}_{jt,\mathrm{e}}} \right), \quad (8)$$

where $\boldsymbol{\Psi}_{mjt} = J \rho_{\mathrm{p}} \sum_{t \in \mathcal{T}} \boldsymbol{R}_{mjt} + \sigma^2 \boldsymbol{I}_N$, $\boldsymbol{R}_{mjt} = \beta_{mjt} \tilde{\boldsymbol{R}}_{mjt}$, $\boldsymbol{\Psi}_{jt,\mathrm{e}} = J \rho_{\mathrm{p}} \sum_{t \in \mathcal{T}} \boldsymbol{R}_{jt,\mathrm{e}} + \sigma^2 \boldsymbol{I}_L$ and $\boldsymbol{R}_{jt,\mathrm{e}} = \beta_{jt,\mathrm{e}} \tilde{\boldsymbol{R}}_{jt,\mathrm{e}}$.

III. Uplink Data Transmission

In this section, we establish the received data signals at the APs, CPU, and Eve under different multiple access protocols[2].

A. Data Transmission for RSMA

In the context of RSMA, user k splits its message w_k into two components, w_{k1} and w_{k2}, which are then independently encoded into two uncorrelated streams, s_{k1} and s_{k2}, with unit variance. To control the transmission power for these streams, user k employs two power control coefficients, ξ_{k1} and ξ_{k2}, satisfying $\xi_{k1} + \xi_{k2} \leqslant 1$. Assuming all users simultaneously transmit their data streams to the APs under a maximum power

[1]It is assumed that Eve has access to the pilots of the users and employs MMSE estimation to estimate $\boldsymbol{g}_{k,\mathrm{e}}, \forall k \in \mathcal{K}$. This assumption reflects a worst-case scenario, enhancing Eve's decoding capabilities.

[2]To maintain clarity in the paper's organization, the theoretical analysis framework for SDMA is omitted in Sections III and IV, as SDMA can be regarded as a special case of RSMA where no rate splitting or SIC is applied.

constraint ρ_{u}, the superimposed data signal received at AP m can be expressed as

$$\boldsymbol{y}_m = \sqrt{\rho_{\mathrm{u}}} \sum_{k\in\mathcal{K}} \boldsymbol{g}_{mk} \left(\sqrt{\xi_{k1}} s_{k1} + \sqrt{\xi_{k2}} s_{k2} \right) + \boldsymbol{n}_m, \quad (9)$$

where $\boldsymbol{n}_m \sim \mathcal{N}_{\mathbb{C}} (\boldsymbol{0}_N, \boldsymbol{I}_N)$ is the AWGN. To detect the desired message, AP m first employs $\hat{\boldsymbol{g}}_{mk}^H$ to decouple $\boldsymbol{y}_m$ and then forwards the decoupled $\alpha_{mk} \hat{\boldsymbol{g}}_{mk}^H \boldsymbol{y}_m$ to the central processing unit for further detection, where α_{mk} is the weighting factor. Hence, the aggregated received signal at the CPU is given as

$$\begin{aligned} r_k = \sqrt{\rho_{\mathrm{u}}} \sum_{m\in\mathcal{M}} \alpha_{mk} \hat{\boldsymbol{g}}_{mk}^H \boldsymbol{g}_{mk} \left(\sqrt{\xi_{k1}} s_{k1} + \sqrt{\xi_{k2}} s_{k2} \right) \\ + \sqrt{\rho_{\mathrm{u}}} \sum_{k'\in\mathcal{K}\setminus\{k\}} \sum_{m\in\mathcal{M}} \alpha_{mk} \hat{\boldsymbol{g}}_{mk}^H \boldsymbol{g}_{mk'} \left(\sqrt{\xi_{k'1}} s_{k'1} + \sqrt{\xi_{k'2}} s_{k'2} \right) \\ + \sum_{m\in\mathcal{M}} \alpha_{mk} \hat{\boldsymbol{g}}_{mk}^H \boldsymbol{n}_m. \end{aligned} \quad (10)$$

Similarly, the received data signal at Eve is expressed as

$$\begin{aligned} r_{k,\mathrm{e}} = \sqrt{\rho_{\mathrm{u}}} \hat{\boldsymbol{g}}_{k,\mathrm{e}}^H \boldsymbol{g}_{k,\mathrm{e}} \left(\sqrt{\xi_{k1}} s_{k1} + \sqrt{\xi_{k2}} s_{k2} \right) + \hat{\boldsymbol{g}}_{k,\mathrm{e}}^H \boldsymbol{n}_{\mathrm{e}} \\ + \sqrt{\rho_{\mathrm{u}}} \sum_{k'\in\mathcal{K}\setminus\{k\}} \hat{\boldsymbol{g}}_{k,\mathrm{e}}^H \boldsymbol{g}_{k',\mathrm{e}} \left(\sqrt{\xi_{k'1}} s_{k'1} + \sqrt{\xi_{k'2}} s_{k'2} \right), \end{aligned} \quad (11)$$

where $\boldsymbol{n}_{\mathrm{e}} \sim \mathcal{N}_{\mathbb{C}} (\boldsymbol{0}_L, \boldsymbol{I}_L)$ denotes the AWGN at Eve.

B. Data Transmission for NOMA

Denote q_{jt} as the data stream of user jt and η_{jt} as the corresponding power control coefficient, the aggregated signal received at AP m is represented as

$$\boldsymbol{x}_m = \sqrt{\rho_{\mathrm{u}}} \sum_{j\in\mathcal{J}} \sum_{t\in\mathcal{T}} \sqrt{\eta_{jt}} \boldsymbol{g}_{mjt} q_{jt} + \boldsymbol{w}_m, \quad (12)$$

where $\boldsymbol{w}_m \sim \mathcal{N}_{\mathbb{C}} (\boldsymbol{0}_N, \boldsymbol{I}_N)$ signifies the AWGN. Using the decoding method adopted in RSMA, the superposition of all data signals received at the CPU can be expressed as

$$\begin{aligned} z_{jt} = \sqrt{\rho_{\mathrm{u}} \eta_{jt}} \sum_{m\in\mathcal{M}} \alpha_{mjt} \hat{\boldsymbol{g}}_{mjt}^H \boldsymbol{g}_{mjt} q_{jt} + \sum_{m\in\mathcal{M}} \alpha_{mjt} \hat{\boldsymbol{g}}_{mjt}^H \boldsymbol{w}_m \\ + \sqrt{\rho_{\mathrm{u}}} \sum_{j'\in\mathcal{J}\setminus\{j\}} \sum_{t\in\mathcal{T}} \sqrt{\eta_{j't'}} \sum_{m\in\mathcal{M}} \alpha_{mjt} \hat{\boldsymbol{g}}_{mjt}^H \boldsymbol{g}_{mj't'} q_{j't'} \\ + \sqrt{\rho_{\mathrm{u}}} \sum_{t'\in\mathcal{T}\setminus\{t\}} \sqrt{\eta_{jt'}} \sum_{m\in\mathcal{M}} \alpha_{mjt} \hat{\boldsymbol{g}}_{mjt}^H \boldsymbol{g}_{mjt'} q_{jt'}, \end{aligned} \quad (13)$$

where α_{mjt} is the weighting factor. In a similar vein, the received data signal at Eve is given as

$$\begin{aligned} z_{jt,\mathrm{e}} = \sqrt{\rho_{\mathrm{u}} \eta_{jt}} \hat{\boldsymbol{g}}_{jt,\mathrm{e}}^H \boldsymbol{g}_{mjt} q_{jt} + \sqrt{\rho_{\mathrm{u}}} \sum_{t'\in\mathcal{T}\setminus\{t\}} \sqrt{\eta_{jt'}} \hat{\boldsymbol{g}}_{jt,\mathrm{e}}^H \boldsymbol{g}_{jt',\mathrm{e}} q_{jt'} \\ + \sqrt{\rho_{\mathrm{u}}} \sum_{j'\in\mathcal{J}\setminus\{j\}} \sum_{t\in\mathcal{T}} \sqrt{\eta_{j't'}} \hat{\boldsymbol{g}}_{jt,\mathrm{e}}^H \boldsymbol{g}_{j't',\mathrm{e}} q_{j't'} + \hat{\boldsymbol{g}}_{jt,\mathrm{e}}^H \boldsymbol{w}_{\mathrm{e}}, \end{aligned} \quad (14)$$

where $\boldsymbol{w}_{\mathrm{e}} \sim \mathcal{N}_{\mathbb{C}} (\boldsymbol{0}_L, \boldsymbol{I}_L)$ denotes the AWGN.

IV. Closed-Form Secrecy Spectral Efficiency Analysis

In this section, we derive tight closed-form formulas for the achievable legitimate, leakage, and secrecy SEs for both RSMA and NOMA protocols by employing the use-and-then-forget (UatF) bounding technique [2].

A. Legitimate, Leakage, and Secrecy SEs for RSMA

RSMA allows the implementation of SIC to cancel the data streams of users k' with $k' < k$. By applying the UatF bound technique to (10), the first stream decoded at the CPU for user k is given as (15). We can treat the last five terms on the right-hand side (RHS) of (15) as effective noise and prove that they are uncorrelated with the desired signal. Once the first stream of user k is decoded, the second part of user k's received signal is written as (16). Similarly, the last three terms on the RHS of (16) can be treated as effective noise, which are uncorrelated with the desired signal. Next, by applying the worst-case Gaussian argument [2], the achievable signal-to-interference-plus-noise ratios (SINRs) for user k when decoding s_{k1} and s_{k2} based on (15) and (16) are formulated as (17) and (18), respectively. After computing all expected values in (17) and (18), Proposition 1 provides the closed-form expression for the legitimate SE of user k.

Proposition 1: Assuming RSMA, the closed-form legitimate SE of user k is given by $\mathcal{R}_k^{\mathrm{RS}} = \mathcal{R}_{k1}^{\mathrm{RS}} + \mathcal{R}_{k2}^{\mathrm{RS}}$, where $\mathcal{R}_{k1}^{\mathrm{RS}}$ and $\mathcal{R}_{k2}^{\mathrm{RS}}$ are the legitimate SEs regarding the first and second streams of user k, respectively shown as

$$\mathcal{R}_{k1}^{\mathrm{RS}} = \tfrac{\tau_{\mathrm{c}} - \tau_{\mathrm{p}}}{\tau_{\mathrm{c}}} \log_2 \left(1 + \frac{\xi_{k1} \boldsymbol{\alpha}_k^H \boldsymbol{\gamma}_{kk} \boldsymbol{\gamma}_{kk}^H \boldsymbol{\alpha}_k}{\boldsymbol{\alpha}_k^H \boldsymbol{\Phi}_{k1} \boldsymbol{\alpha}_k} \right), \quad (19)$$

$$\mathcal{R}_{k2}^{\mathrm{RS}} = \tfrac{\tau_{\mathrm{c}} - \tau_{\mathrm{p}}}{\tau_{\mathrm{c}}} \log_2 \left(1 + \frac{\xi_{k2} \boldsymbol{\alpha}_k^H \boldsymbol{\gamma}_{kk} \boldsymbol{\gamma}_{kk}^H \boldsymbol{\alpha}_k}{\boldsymbol{\alpha}_k^H \boldsymbol{\Phi}_{k2} \boldsymbol{\alpha}_k} \right), \quad (20)$$

where τ_{c} represents the length of the coherence interval, $\boldsymbol{\alpha}_k = [\alpha_{1k}, ..., \alpha_{Mk}]^T \in \mathbb{C}^M$, $\boldsymbol{\gamma}_{kk} = [\gamma_{1kk}, ..., \gamma_{Mkk}]^T \in \mathbb{C}^M$, $\boldsymbol{\Delta}_{kk'} = \mathrm{diag} \{\delta_{1kk'}, ..., \delta_{Mkk'}\} \in \mathbb{C}^{M\times M}$, $\boldsymbol{\Phi}_{k2} = \boldsymbol{\Phi}_{k1} - \xi_{k2} \boldsymbol{\gamma}_{kk} \boldsymbol{\gamma}_{kk}^H$, and

$$\begin{aligned} \boldsymbol{\Phi}_{k1} = \sum_{k'\in\mathcal{K}, k'>k} (\xi_{k'1} + \xi_{k'2}) \left(\boldsymbol{\Delta}_{kk'} + \boldsymbol{\gamma}_{kk'} \boldsymbol{\gamma}_{kk'}^H \right) + \tfrac{1}{\rho_{\mathrm{u}}} \mathrm{diag} \{\boldsymbol{\gamma}_{kk}\} \\ + \sum_{k'\in\mathcal{K}, k'\leqslant k} (\xi_{k'1} + \xi_{k'2}) \boldsymbol{\Delta}_{kk'} + \xi_{k2} \boldsymbol{\gamma}_{kk} \boldsymbol{\gamma}_{kk}^H, \end{aligned} \quad (21)$$

$$\gamma_{mkk'} = \mathrm{Tr} \left[e^{i \left(\theta_{mk'}^{\mathrm{P}} - \theta_{mk}^{\mathrm{P}} \right)} \bar{\boldsymbol{h}}_{mk'} \bar{\boldsymbol{h}}_{mk}^H + \left| \boldsymbol{\varphi}_{k'}^H \boldsymbol{\varphi}_k \right| \boldsymbol{Q}_{mk} \boldsymbol{R}_{mk}^{-1} \boldsymbol{R}_{mk'} \right], \quad (22)$$

$$\delta_{mkk'} = \mathrm{Tr} \left[\boldsymbol{Q}_{mk} \boldsymbol{R}_{mk'} \right] + \bar{\boldsymbol{h}}_{mk}^H \boldsymbol{R}_{mk'} \bar{\boldsymbol{h}}_{mk} + \bar{\boldsymbol{h}}_{mk'}^H \boldsymbol{Q}_{mk} \bar{\boldsymbol{h}}_{mk'}. \quad (23)$$

Turning our attention to Eve, we assume that it operates as a typical user with limited demodulation capabilities, which prevent it from canceling any interference [11]. Consequently, SIC cannot be applied to (11). Using the same methodology employed in deriving the legitimate SE for user k, Proposition 2 provides the closed-form expressions for the leakage SE when Eve intercepts the data signal of user k.

Proposition 2: Assuming RSMA, the closed-form leakage SE formula when Eve wiretaps the data stream of user k is written as $\mathcal{R}_{k,\mathrm{e}}^{\mathrm{RS}} = \mathcal{R}_{k1,\mathrm{e}}^{\mathrm{RS}} + \mathcal{R}_{k2,\mathrm{e}}^{\mathrm{RS}}$, where $\mathcal{R}_{k1,\mathrm{e}}^{\mathrm{RS}}$ and $\mathcal{R}_{k2,\mathrm{e}}^{\mathrm{RS}}$ are the leakage SEs regarding the first and second data streams of user k, as shown in (24) and (25), respectively, where

$$\gamma_{kk',\mathrm{e}} = \mathrm{Tr} \left[e^{i \left(\theta_{k',\mathrm{e}}^{\mathrm{P}} - \theta_{k,\mathrm{e}}^{\mathrm{P}} \right)} \bar{\boldsymbol{h}}_{k',\mathrm{e}} \bar{\boldsymbol{h}}_{k,\mathrm{e}}^H + \left| \boldsymbol{\varphi}_{k'}^H \boldsymbol{\varphi}_k \right| \boldsymbol{Q}_{k,\mathrm{e}} \boldsymbol{R}_{k,\mathrm{e}}^{-1} \boldsymbol{R}_{k',\mathrm{e}} \right], \quad (26)$$

$$\delta_{kk',\mathrm{e}} = \mathrm{Tr} \left[\boldsymbol{Q}_{k,\mathrm{e}} \boldsymbol{R}_{k',\mathrm{e}} \right] + \bar{\boldsymbol{h}}_{k,\mathrm{e}}^H \boldsymbol{R}_{k',\mathrm{e}} \bar{\boldsymbol{h}}_{k,\mathrm{e}} + \bar{\boldsymbol{h}}_{k',\mathrm{e}}^H \boldsymbol{Q}_{k,\mathrm{e}} \bar{\boldsymbol{h}}_{k',\mathrm{e}}. \quad (27)$$

Based on Propositions 1 and 2, the SSE of user k is given

$$r_{k1} = \sqrt{\rho_{\mathrm{u}}}\xi_{k1}\sum_{m\in\mathcal{M}}\alpha_{mk}\mathbb{E}\left\{\hat{\boldsymbol{g}}_{mk}^H\boldsymbol{g}_{mk}\right\}s_{k1} + \sqrt{\rho_{\mathrm{u}}}\xi_{k2}\sum_{m\in\mathcal{M}}\alpha_{mk}\hat{\boldsymbol{g}}_{mk}^H\boldsymbol{g}_{mk}s_{k2}$$
$$+\sqrt{\rho_{\mathrm{u}}}\xi_{k1}\sum_{m\in\mathcal{M}}\alpha_{mk}\left(\hat{\boldsymbol{g}}_{mk}^H\boldsymbol{g}_{mk} - \mathbb{E}\left\{\hat{\boldsymbol{g}}_{mk}^H\boldsymbol{g}_{mk}\right\}\right)s_{k1} + \sqrt{\rho_{\mathrm{u}}}\sum_{k'\in\mathcal{K},k'>k}\sum_{m\in\mathcal{M}}\alpha_{mk}\hat{\boldsymbol{g}}_{mk}^H\boldsymbol{g}_{mk'}\left(\sqrt{\xi_{k'1}}s_{k'1}+\sqrt{\xi_{k'2}}s_{k'2}\right)$$
$$+\sqrt{\rho_{\mathrm{u}}}\sum_{k'\in\mathcal{K},k'<k}\sum_{m\in\mathcal{M}}\alpha_{mk}\left(\hat{\boldsymbol{g}}_{mk}^H\boldsymbol{g}_{mk'} - \mathbb{E}\left\{\hat{\boldsymbol{g}}_{mk}^H\boldsymbol{g}_{mk'}\right\}\right)\left(\sqrt{\xi_{k'1}}s_{k'1}+\sqrt{\xi_{k'2}}s_{k'2}\right) + \sum_{m\in\mathcal{M}}\alpha_{mk}\hat{\boldsymbol{g}}_{mk}^H\boldsymbol{n}_m. \quad (15)$$

$$r_{k2} = \sqrt{\rho_{\mathrm{u}}}\xi_{k2}\sum_{m\in\mathcal{M}}\alpha_{mk}\mathbb{E}\left\{\hat{\boldsymbol{g}}_{mk}^H\boldsymbol{g}_{mk}\right\}s_{k2} + \sqrt{\rho_{\mathrm{u}}}\sum_{k'\in\mathcal{K},k'>k}\sum_{m\in\mathcal{M}}\alpha_{mk}\hat{\boldsymbol{g}}_{mk}^H\boldsymbol{g}_{mk'}\left(\sqrt{\xi_{k'1}}s_{k'1}+\sqrt{\xi_{k'2}}s_{k'2}\right)$$
$$+\sqrt{\rho_{\mathrm{u}}}\sum_{k'\in\mathcal{K},k'\leqslant k}\sum_{m\in\mathcal{M}}\alpha_{mk}\left(\hat{\boldsymbol{g}}_{mk}^H\boldsymbol{g}_{mk'} - \mathbb{E}\left\{\hat{\boldsymbol{g}}_{mk}^H\boldsymbol{g}_{mk'}\right\}\right)\left(\sqrt{\xi_{k'1}}s_{k'1}+\sqrt{\xi_{k'2}}s_{k'2}\right) + \sum_{m\in\mathcal{M}}\alpha_{mk}\hat{\boldsymbol{g}}_{mk}^H\boldsymbol{n}_m. \quad (16)$$

$$\mathrm{SINR}_{k1} = \frac{\xi_{k1}\left|\sum_{m\in\mathcal{M}}\alpha_{mk}\mathbb{E}\left\{\hat{\boldsymbol{g}}_{mk}^H\boldsymbol{g}_{mk}\right\}\right|^2}{\left(\begin{array}{l}\xi_{k1}\mathrm{Var}\left\{\sum_{m\in\mathcal{M}}\alpha_{mk}\hat{\boldsymbol{g}}_{mk}^H\boldsymbol{g}_{mk}\right\} + \xi_{k2}\mathbb{E}\left\{\left|\sum_{m\in\mathcal{M}}\alpha_{mk}\hat{\boldsymbol{g}}_{mk}^H\boldsymbol{g}_{mk}\right|^2\right\} + \frac{1}{\rho_{\mathrm{u}}}\mathbb{E}\left\{\left|\sum_{m\in\mathcal{M}}\alpha_{mk}\hat{\boldsymbol{g}}_{mk}^H\boldsymbol{n}_m\right|^2\right\}\\ +\sum_{k'\in\mathcal{K},k'<k}(\xi_{k'1}+\xi_{k'2})\,\mathrm{Var}\left\{\sum_{m\in\mathcal{M}}\alpha_{mk}\hat{\boldsymbol{g}}_{mk}^H\boldsymbol{g}_{mk'}\right\} + \sum_{k'\in\mathcal{K},k'>k}(\xi_{k'1}+\xi_{k'2})\,\mathbb{E}\left\{\left|\sum_{m\in\mathcal{M}}\alpha_{mk}\hat{\boldsymbol{g}}_{mk}^H\boldsymbol{g}_{mk'}\right|^2\right\}\end{array}\right)}. \quad (17)$$

$$\mathrm{SINR}_{k2} = \frac{\xi_{k2}\left|\mathbb{E}\left\{\sum_{m\in\mathcal{M}}\alpha_{mk}\hat{\boldsymbol{g}}_{mk}^H\boldsymbol{g}_{mk}\right\}\right|^2}{\left(\begin{array}{l}\sum_{k'\in\mathcal{K},k'\leqslant k}(\xi_{k'1}+\xi_{k'2})\,\mathrm{Var}\left\{\sum_{m\in\mathcal{M}}\alpha_{mk}\hat{\boldsymbol{g}}_{mk}^H\boldsymbol{g}_{mk'}\right\} + \frac{1}{\rho_{\mathrm{u}}}\mathbb{E}\left\{\left|\sum_{m\in\mathcal{M}}\alpha_{mk}\hat{\boldsymbol{g}}_{mk}^H\boldsymbol{n}_m\right|^2\right\}\\ +\sum_{k'\in\mathcal{K},k'>k}(\xi_{k'1}+\xi_{k'2})\,\mathbb{E}\left\{\left|\sum_{m\in\mathcal{M}}\alpha_{mk}\hat{\boldsymbol{g}}_{mk}^H\boldsymbol{g}_{mk'}\right|^2\right\}\end{array}\right)}. \quad (18)$$

$$\mathcal{R}_{k1,\mathrm{e}}^{\mathrm{RS}} = \tfrac{\tau_{\mathrm{c}}-\tau_{\mathrm{p}}}{\tau_{\mathrm{c}}}\log_2\left(1+\frac{\xi_{k1}\gamma_{kk,\mathrm{e}}^2}{\sum_{k'\in\mathcal{K},k'>k}(\xi_{k'1}+\xi_{k'2})\left(\delta_{kk',\mathrm{e}}+\gamma_{kk',\mathrm{e}}^2\right)+\sum_{k'\in\mathcal{K},k'\leqslant k}(\xi_{k'1}+\xi_{k'2})\,\delta_{kk',\mathrm{e}}+\xi_{k2}\gamma_{kk,\mathrm{e}}^2+\frac{1}{\rho_{\mathrm{u}}}\gamma_{kk,\mathrm{e}}}\right), \quad (24)$$

$$\mathcal{R}_{k2,\mathrm{e}}^{\mathrm{RS}} = \tfrac{\tau_{\mathrm{c}}-\tau_{\mathrm{p}}}{\tau_{\mathrm{c}}}\log_2\left(1+\frac{\xi_{k2}\gamma_{kk,\mathrm{e}}^2}{\sum_{k'\in\mathcal{K},k'>k}(\xi_{k'1}+\xi_{k'2})\left(\delta_{kk',\mathrm{e}}+\gamma_{kk',\mathrm{e}}^2\right)+\sum_{k'\in\mathcal{K},k'\leqslant k}(\xi_{k'1}+\xi_{k'2})\,\delta_{kk',\mathrm{e}}+\xi_{k1}\gamma_{kk,\mathrm{e}}^2+\frac{1}{\rho_{\mathrm{u}}}\gamma_{kk,\mathrm{e}}}\right). \quad (25)$$

as $\mathcal{R}_{k,\mathrm{s}}^{\mathrm{RS}} = \max\left(0, \mathcal{R}_{k}^{\mathrm{RS}} - \mathcal{R}_{k,\mathrm{e}}^{\mathrm{RS}}\right)$.

B. Legitimate, Leakage, and Secrecy SEs for NOMA

For uplink NOMA, the decoding order prioritizes the user with superior channel conditions over the one with inferior channel propagation. By applying SIC and UatF bounding techniques to (13), we obtain (28). Similarly, under the worst-case Gaussian assumption, the achievable SINR for user jt when decoding q_{jt} based on (28) is given by (29). After evaluating all expected values in (29), Proposition 3 establishes the legitimate SE of user k.

Proposition 3: Assuming NOMA, the closed-form legitimate SE formula of user jt is expressed as

$$\mathcal{R}_{jt}^{\mathrm{NO}} = \tfrac{\tau_{\mathrm{c}}-J}{\tau_{\mathrm{c}}}\log_2\left(1+\frac{\eta_{jt}\boldsymbol{\alpha}_{jt}^H\boldsymbol{\gamma}_{jt,jt}\boldsymbol{\gamma}_{jt,jt}^H\boldsymbol{\alpha}_{jt}}{\boldsymbol{\alpha}_{jt}^H\boldsymbol{\Phi}_{jt}\boldsymbol{\alpha}_{jt}}\right), \quad (30)$$

where $\boldsymbol{\alpha}_{jt} = [\alpha_{1jt},...,\alpha_{Mjt}]^T \in \mathbb{C}^M$, $\boldsymbol{\gamma}_{jt,jt} = [\gamma_{1jt,jt},..., \gamma_{Mjt,jt}]^T \in \mathbb{C}^M$, $\boldsymbol{\Delta}_{jt,j't'} = \mathrm{diag}\left\{\delta_{1jt,j't'},...,\delta_{Mjt,j't'}\right\}$, and

$$\boldsymbol{\Phi}_{jt,j't'} = \sum_{k'\in\mathcal{T},t'>t}\eta_{jt'}\left(\boldsymbol{\Delta}_{jt,jt'}+\boldsymbol{\gamma}_{jt,jt'}\boldsymbol{\gamma}_{jt,jt'}^H\right) + \sum_{t'\in\mathcal{T},t'\leqslant t}\eta_{jt'}\boldsymbol{\Delta}_{jt,jt'} + \tfrac{1}{\rho_{\mathrm{u}}}\mathrm{diag}\left\{\boldsymbol{\gamma}_{jt,jt}\right\} + \sum_{j'\in\mathcal{J}\setminus\{j\}}\sum_{t\in\mathcal{T}}\eta_{j't'}\left(\boldsymbol{\Delta}_{jt,j't'}+\boldsymbol{\gamma}_{jt,j't'}\boldsymbol{\gamma}_{jt,j't'}^H\right), \quad (31)$$

$$\boldsymbol{\gamma}_{mjt,j't'} = \mathrm{Tr}\left[e^{i\left(\theta_{mj't'}^{\mathrm{P}}-\theta_{mjt}^{\mathrm{P}}\right)}\bar{\boldsymbol{h}}_{mj't'}\bar{\boldsymbol{h}}_{mjt}^H\right] + \mathrm{Tr}\left[\left|\boldsymbol{\varphi}_{j'}^H\boldsymbol{\varphi}_j\right|\boldsymbol{Q}_{mjt}\boldsymbol{R}_{mjt}^{-1}\boldsymbol{R}_{mj't'}\right]. \quad (32)$$

and

$$\delta_{mjt,j't'} = \mathrm{Tr}\left[\boldsymbol{Q}_{mjt}\boldsymbol{R}_{mj't'}\right] + \bar{\boldsymbol{h}}_{mjt}^H\boldsymbol{R}_{mj't'}\bar{\boldsymbol{h}}_{mjt} + \bar{\boldsymbol{h}}_{mj't'}^H\boldsymbol{Q}_{mjt}\bar{\boldsymbol{h}}_{mj't'}. \quad (33)$$

$$z_{jt} = \sqrt{\rho_{\mathrm{u}}\eta_{jt}} \sum_{m\in\mathcal{M}} \alpha_{mjt}\mathbb{E}\left\{\hat{\boldsymbol{g}}_{mjt}^H \boldsymbol{g}_{mjt}\right\} q_{jt} + \sqrt{\rho_{\mathrm{u}}\eta_{jt}} \sum_{m\in\mathcal{M}} \alpha_{mjt}\left(\hat{\boldsymbol{g}}_{mjt}^H \boldsymbol{g}_{mjt} - \mathbb{E}\left\{\hat{\boldsymbol{g}}_{mjt}^H \boldsymbol{g}_{mjt}\right\}\right) q_{jt}$$
$$+ \sqrt{\rho_{\mathrm{u}}} \sum_{t'\in\mathcal{T},t'<t} \sqrt{\eta_{jt'}} \sum_{m\in\mathcal{M}} \alpha_{mjt}\left(\hat{\boldsymbol{g}}_{mjt}^H \boldsymbol{g}_{mjt'} - \mathbb{E}\left\{\hat{\boldsymbol{g}}_{mjt}^H \boldsymbol{g}_{mjt'}\right\}\right) q_{jt'} + \sum_{m\in\mathcal{M}} \alpha_{mjt}\hat{\boldsymbol{g}}_{mjt}^H \boldsymbol{w}_m$$
$$+ \sqrt{\rho_{\mathrm{u}}} \sum_{t'\in\mathcal{T},t'>t} \sqrt{\eta_{jt'}}\mathbb{E}\left\{\sum_{m\in\mathcal{M}} \alpha_{mjt}\hat{\boldsymbol{g}}_{mjt}^H \boldsymbol{g}_{mjt'}\right\} q_{jt'} + \sqrt{\rho_{\mathrm{u}}} \sum_{j'\in\mathcal{J}\setminus\{j\}} \sum_{t\in\mathcal{T}} \sqrt{\eta_{j't'}}\mathbb{E}\left\{\sum_{m\in\mathcal{M}} \alpha_{mjt}\hat{\boldsymbol{g}}_{mjt}^H \boldsymbol{g}_{mj't'}\right\} q_{j't'}. \quad (28)$$

$$\mathrm{SINR}_{jt} = \frac{\eta_{jt}\left|\sum_{m\in\mathcal{M}} \alpha_{mjt}\mathbb{E}\left\{\hat{\boldsymbol{g}}_{mjt}^H \boldsymbol{g}_{mjt}\right\}\right|^2}{\left(\begin{array}{l}\sum_{t'\in\mathcal{T},t'\leqslant t} \eta_{jt'}\mathrm{Var}\left\{\sum_{m\in\mathcal{M}} \alpha_{mjt}\hat{\boldsymbol{g}}_{mjt}^H \boldsymbol{g}_{mjt'}\right\} + \sum_{t'\in\mathcal{T},t'>t} \eta_{jt'}\left|\mathbb{E}\left\{\sum_{m\in\mathcal{M}} \alpha_{mjt}\hat{\boldsymbol{g}}_{mjt}^H \boldsymbol{g}_{mjt'}\right\}\right|^2 \\ \sum_{j'\in\mathcal{J}\setminus\{j\}} \sum_{t\in\mathcal{T}} \eta_{j't'}\left|\mathbb{E}\left\{\sum_{m\in\mathcal{M}} \alpha_{mjt}\hat{\boldsymbol{g}}_{mjt}^H \boldsymbol{g}_{mj't'}\right\}\right|^2 + \frac{1}{\rho_{\mathrm{u}}}\mathbb{E}\left\{\left|\sum_{m\in\mathcal{M}} \alpha_{mjt}\hat{\boldsymbol{g}}_{mjt}^H \boldsymbol{w}_m\right|^2\right\}\end{array}\right)}. \quad (29)$$

$$\mathcal{R}_{jt,\mathrm{e}}^{\mathrm{NO}} = \frac{\tau_{\mathrm{c}}-J}{\tau_{\mathrm{c}}}\log_2\left(1 + \frac{\eta_{jt}\gamma_{jt,jt,\mathrm{e}}^2}{\sum_{t'\in\mathcal{T}\setminus\{t\}} \eta_{jt'}\left(\delta_{jt,jt',\mathrm{e}} + \gamma_{jt,jt',\mathrm{e}}^2\right) + \sum_{j'\in\mathcal{J}\setminus\{j\}} \sum_{t'\in\mathcal{T}} \eta_{j't'}\left(\delta_{jt,j't',\mathrm{e}} + \gamma_{jt,j't',\mathrm{e}}^2\right) + \eta_{jt}\delta_{jt,jt,\mathrm{e}} + \frac{1}{\rho_{\mathrm{u}}}\gamma_{jt,jt,\mathrm{e}}}\right). \quad (34)$$

By applying a similar approach used to derive the legitimate SE of user jt, Proposition 4 presents a closed-form expression for the leakage SE when Eve wiretaps the signal of user jt.

Proposition 4: Assuming NOMA, the closed-form leakage SE formula when Eve wiretaps the data stream of user jt is written as (34), where

$$\gamma_{jt,j't',\mathrm{e}} = \mathrm{Tr}\left[e^{i\left(\theta_{j't',\mathrm{e}}^{\mathrm{P}} - \theta_{jt,\mathrm{e}}^{\mathrm{P}}\right)}\bar{\boldsymbol{h}}_{j't',\mathrm{e}}\bar{\boldsymbol{h}}_{jt,\mathrm{e}}^H\right] + \mathrm{Tr}\left[\left|\boldsymbol{\varphi}_{j'}^H\boldsymbol{\varphi}_j\right|\boldsymbol{Q}_{jt,\mathrm{e}}\boldsymbol{R}_{jt,\mathrm{e}}^{-1}\boldsymbol{R}_{j't',\mathrm{e}}\right], \quad (35)$$

and

$$\delta_{jt,j't',\mathrm{e}} = \mathrm{Tr}\left[\boldsymbol{Q}_{jt,\mathrm{e}}\boldsymbol{R}_{j't',\mathrm{e}}\right] + \bar{\boldsymbol{h}}_{jt,\mathrm{e}}^H\boldsymbol{R}_{j't',\mathrm{e}}\bar{\boldsymbol{h}}_{jt,\mathrm{e}} + \bar{\boldsymbol{h}}_{j't',\mathrm{e}}^H\boldsymbol{Q}_{jt,\mathrm{e}}\bar{\boldsymbol{h}}_{j't',\mathrm{e}}. \quad (36)$$

Based on Propositions 3 and 4, the SSE of user jt under NOMA is given as $\mathcal{R}_{jt,\mathrm{s}}^{\mathrm{NO}} = \max\left(0, \mathcal{R}_{jt}^{\mathrm{NO}} - \mathcal{R}_{jt,\mathrm{e}}^{\mathrm{NO}}\right)$.

V. Simulation Results and Discussions

This section presents comprehensive simulations to evaluate and compare the SSEs of RSMA, SDMA, and NOMA protocols.

A. Parameter Setups

In our work, all the APs and users are uniformly distributed throughout an urban area measuring 1000×1000 m^2, with the Eve centrally located within this region. The large-scale fading coefficients between the APs and users, as well as between Eve and users, are generated using the COST 231 Walfish-Ikegami model at a carrier frequency of 1900 MHz [12]. The LoS probabilities, Ricean factors, and spatial correlation matrices are modeled in accordance with [12, (37)] and [10, (46)].

We employ a benchmark with full power control and unitary receiver combination for performance evaluation, i.e., $\xi_{k1} = \xi_{k2} = \frac{1}{2}$, $\eta_{jt} = 1$, and $\alpha_{mjt} = \frac{1}{\sqrt{M}}$. Unless otherwise specified, the simulation parameters are set as follows: $\rho_{\mathrm{u}} = \rho_{\mathrm{p}} = 20$ dBm, $\sigma^2 = -96$ dBm, $\tau_{\mathrm{p}} = J = \frac{K}{4}$, and $\tau = 100$.

B. Performance Evaluation with FPC-URC

Fig. 1 plots the cumulative distribution functions (CDFs) of per-user SSEs for RSMA, SDMA, and NOMA schemes, obtained from 1000 independent channel realizations. The results clearly show that RSMA achieves a superior SSE compared to both NOMA and SDMA, which can be attributed to its enhanced interference management capabilities. As the number of users increases from 9 to 12, a noticeable decline in SSE is observed, with a higher proportion of users experiencing zero SSE. This highlights the increased vulnerability of systems with a larger user number to security risks. Furthermore, the accuracy of the derived closed-form SSE expressions is validated in Fig. 1 by comparing them with Monte-Carlo simulation results. The close agreement between the theoretical and simulated SSE values for both $K = 9$ and $K = 12$ confirms the tightness of the UatF SSE bounds.

Fig. 2 presents the sum SSEs for K ranging from 6 to 30 under varying pilot lengths and fading channel conditions. The sum SSEs are shown to increase with K, with the performance gap between RSMA and NOMA/SDMA widening as K grows, particularly when $\tau_{\mathrm{p}} = J = 3$. This highlights RSMA's robustness against pilot contamination, making it well-suited for scenarios with a larger number of users. Additionally, Fig. 2 demonstrates that NOMA's SSE advantage over SDMA is strongly influenced by the number of NOMA clusters. While extending the pilot reduces pilot contamination, the increased pilot overhead in such cases significantly diminishes the SSE, narrowing the SSE disparity between NOMA and SDMA. As

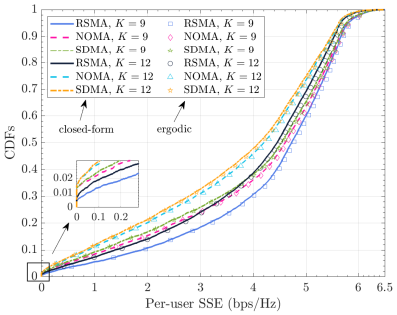

Fig. 1. CDFs of per-user SSEs for RSMA, NOMA, and SDMA protocols. In this simulation, $M=36$, $N=4$, $L=4$, $\tau_{\mathrm{p}}=\frac{K}{3}$.

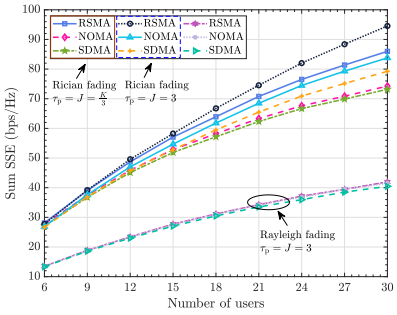

Fig. 2. Sum SSEs for RSMA, NOMA, and SDMA protocols versus the number of users under different fading channels and lengths of pilots. In this simulation, $M=36$, $N=4$, and $L=4$.

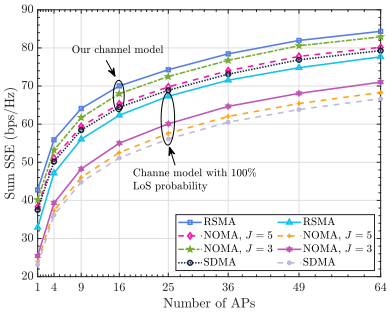

Fig. 3. Sum SSEs for RSMA, NOMA, and SDMA protocols versus the number of APs under pure and mixed LoS assumptions. In this simulation, $K=15$, $N=4$, and $L=4$.

expected, NOMA with $J=3$ outperforms SDMA across all considered K values. Notably, under Rayleigh fading channels, RSMA's performance is comparable to that of NOMA, with both outperforming SDMA by a small margin. This is due to the interference caused by imperfect SIC, which is more pronounced in environments without LoS components, such as Rayleigh fading channels, where the interference is exacerbated by the stochastic nature of the wireless channel.

Fig. 3 explores the impact of varying LoS probabilities on the SSE gains of RSMA over NOMA and SDMA. A channel model with a 100% LoS probability (distance-dependent) is used as a benchmark for comparison with our assumed channel model, which posits that all AP-user and user-Eve pairs have LoS paths. As shown in Fig. 3, the sum SSEs for all schemes increase monotonically with the number of APs, albeit with diminishing returns. This trend arises because increasing AP density reduces the propagation loss between APs and users, while also providing more macro-diversity gains, both of which contribute to improved secrecy performance. Although RSMA consistently outperforms NOMA and SDMA under the assumed channel conditions, its relative advantage is diminished when considering the 100% LoS probability channel model. This suggests that RSMA is particularly well-suited for systems operating in environments with rich LoS paths, aligning with the conclusions drawn from Fig. 2. Interestingly, Fig. 3 also reveals that a 100% LoS probability environment does not necessarily lead to a higher sum SSE, as the enhanced wiretapping capability of Eve in such scenarios offsets the secrecy gains.

VI. Conclusion

This paper investigated the achievable SSE in the uplink of a C-RAN system implementing RSMA, NOMA, and SDMA protocols. Accounting for correlated Rician fading channels and imperfect channel state information, we derived closed-form SSE expressions and performed extensive evaluations based on these theoretical results. Numerical simulations reveal that RSMA, leveraging its adaptive IUI management strategy, demonstrates superior secure transmission capabilities compared to NOMA and SDMA. Moreover, the SSE performance advantage of RSMA becomes particularly pronounced in propagation environments characterized by robust LoS components and severe pilot contamination scenarios.

References

[1] Y. Zhang, W. Xia, H. Zhao, G. Zheng, S. Lambotharan, and L. Yang, "Performance analysis of RIS-assisted cell-free massive MIMO systems with transceiver hardware impairments," *IEEE Trans. Commun.*, vol. 71, no. 12, pp. 7258–7272, Aug. 2023.

[2] H. Q. Ngo, A. Ashikhmin, H. Yang, E. G. Larsson, and T. L. Marzetta, "Cell-free massive MIMO versus small cells," *IEEE Trans. Wirel. Commun.*, vol. 16, no. 3, pp. 1834–1850, Mar. 2017.

[3] Y. Zhang, H.-M. Wang, Q. Yang, and Z. Ding, "Secrecy sum rate maximization in non-orthogonal multiple access," *IEEE Commun. Lett.*, vol. 20, no. 5, pp. 930–933, May 2016.

[4] Y. Zhang, H. Zhao, Y. Mao, W. Xia, W. Lu, and H. Zhu, "Rate-splitting multiple access in cell-free massive MIMO-URLLC systems: Achievable rate analysis and optimization," *IEEE Trans. Commun.*, vol. 72, no. 11, pp. 6752–6767, 2024.

[5] Y. Zhang, H. Zhao, W. Xia, Y. Zhu, H. Q. Ngo, and B. Tan, "Enhancing secrecy in hardware-impaired cell-free massive mimo by rsma," *IEEE Trans. Wirel. Commun.*, pp. 1–18, 2024, early access.

[6] Y. Zhang, W. Xia, G. Zheng, H. Zhao, L. Yang, and H. Zhu, "Secure transmission in cell-free massive MIMO with low-resolution DACs over Rician fading channels," *IEEE Trans. Commun.*, vol. 70, no. 4, pp. 2606–2621, Jan. 2022.

[7] X.-T. Dang, H. V. Nguyen, and O.-S. Shin, "Physical layer security for IRS-UAV-assisted cell-free massive MIMO systems," *IEEE Access*, vol. 12, pp. 89 520–89 537, June 2024.

[8] S. Rivetti, E. Björnson, and M. Skoglund, "Secure spatial signal design for ISAC in a cell-free MIMO network," in *Proc. 2024 IEEE Wireless Communications Networking Conf. (WCNC)*, July 2024, pp. 1–6.

[9] Y. Zhang, K. Yang, W. Xia, J. Zhang, Y. Ni, and W. Lu, "Secure RSMA for CF-mMIMO systems with low-resolution DACs," *IEEE Wirel. Commun. Lett.*, vol. 13, no. 6, pp. 1660–1664, June 2024.

[10] Y. Zhang, W. Xia, H. Zhao, Y. Zhu, W. Xu, and W. Lu, "Performance analysis of cell-free massive MIMO-URLLC systems over correlated Rician fading channels with phase shifts," *IEEE Trans. Wirel. Commun.*, vol. 23, no. 9, pp. 12 206–12 222, Sept. 2024.

[11] Z. Xiang, W. Yang, Y. Cai, Y. Cheng, H. Wu, and M. Wang, "Secrecy performance analysis of uplink NOMA in IoT networks," in *Proc. 2018 IEEE/CIC Int. Conf. Commun. Chin. (ICCC)*, Aug. 2018, pp. 506–510.

[12] Ö. Özdogan, E. Björnson, and J. Zhang, "Cell-free massive MIMO with Rician fading: Estimation schemes and spectral efficiency," in *Proc. 2018 52nd Asilomar Conf. Signals, Syst. Comput. (ACSSC)*, Oct. 2018, pp. 975–979.